JOURNAL OF MATERIALS SCIENCE 14 (1979) 2053–2073

The defect structure of MgO containing trivalent cation solutes: shell model calculations

W. H. GOURDIN*, W. D. KINGERY
Ceramics Division, Department of Materials Science and Engineering, Massachusetts Institute of Technology, Cambridge, Massachusetts 02139, USA

We have used the HADES program to calculate the energies of various defect aggregates found in MgO containing Al^{3+} and Fe^{3+} solutes and compensating cation vacancies. Calculated energies of substitution are compared with heats of solution derived from phase-diagram data; from the accuracy of these results, we deduce the validity of the models used for the lattice simulations. We find that our models provide a satisfactory description for Al^{3+} but are a less precise representation of crystals containing Fe^{3+}; the models used, however, bracket a reasonable range of solute behaviour and important trends are unaffected by reasonable changes in the interionic potentials. The simplest vacancy–solute dimer can have either a ⟨100⟩ or ⟨110⟩ orientation; the two constituent defects are closest when the dimer has a ⟨110⟩ axis, but the ⟨100⟩ dimer is more stable because of the large displacement and polarization of the oxygen ion between the trivalent ion and vacancy. Trimers with either orientation are about twice as stable as the corresponding dimers. Complex aggregates of solutes and vacancies, which adopt configurations that form nuclei of the mixed-oxide spinel structure, are even more stable and the stability increases with cluster size. Thus we conclude that such clustering is an important phenomenon at low homologous temperatures. Calculated interstitial formation energies in MgO are large (> 10 eV) and our results for the activation energies for solute motion are of the order of 2 eV.

1. Introduction

A detailed knowledge of defect structures is important for understanding the physical properties of crystalline ceramic materials. It is necessary both to identify the species present and to characterize the equilibria between them. The appropriate equilibrium constants in the usual mass-action formalism depend on the changes of enthalpy and entropy accompanying point-defect creation or aggregation. However, experiments aimed at determining these quantities for oxides of technological importance (in this paper we consider MgO) are difficult to perform and interpret. Thus, even where there exist experimental estimates of defect-associate binding energies, the values are unreliable.

Calculations of the free energies of various plausible defect configurations would aid the interpretation of the properties of imperfect crystals. Such theoretical modelling of materials can, of course, consider various possible defects and defect aggregates and thus indicate which are the significant participants in the defect chemistry. However, the calculation of the non-configurational defect entropies is extremely difficult; it requires the determination of the local vibrational modes of the imperfect lattice. Thus it is only recently that there have been serious attempts at calculations of defect entropies for ionic materials [1]. This lack of reliable entropies is a serious deficiency in theoretical analyses of defect chemistry. However, because the temperature variation of the mass-action equilibrium constants depends only on the defect energies, if as usual both energies and entropies do not themselves depend

*Present address: Western Electric Engineering Research Center, P. O. Box 900, Princeton, New Jersey 08540, USA.
0022–2461/79/092053–21 $04.10/0

explicitly on temperature, then calculated defect energies alone are of great value in interpreting experimental work.

Recent studies [2] have established appropriate models and improved methods for calculating the energies of defects and defect aggregates in ionic materials; this experience is realized in the HADES computer program (Harwell Automatic Defect Evaluation System) of the Theoretical Physics Division of the UKAEA Research Laboratory at Harwell. This paper reports such calculations of the interaction energies of trivalent cation solutes with cation vacancies in MgO. The work has two objectives. First it seeks to provide self-consistent and plausible energies of formation and association of various point-defect configurations where at present none are known. We can compare such results with experimental heats of solution for the trivalent solutes. Such energies can be used in reliable calculations, within the conventional mass-action formalism, of the concentration of many different defects in the MgO crystal as a function of temperature, impurity content and oxygen partial pressure. Second, this study investigates more complex aggregates of impurities and vacancies, with conjectural but plausible configurations inferred from the known structures of mixed spinel oxides of magnesium and trivalent ions. Such complexes may have a profound effect on the overall defect behaviour.

2. Background

There is little doubt that association between charged point defects occurs in magnesia. A variety of impurity–vacancy* centres have been identified which involve anion substitutionals such as F^- [3, 4] and OH^- [5, 6]. Impurity–impurity centres involving pairs of tri- and monovalent substitutionals such as $(Cr_{Mg}^{\cdot} - Li_{Mg}')^{x\dagger}$ have also been suggested [7]. The defect structures produced by the trivalent solutes Al^{3+}, Fe^{3+} and Cr^{3+} and quadrivalent Mn^{4+} are of particular interest, however, either because such solutes are often present in substantial quantities in single-crystal specimens of magnesia (Al^{3+}, Fe^{3+}), or because they are amenable to detailed study with optical and resonance techniques (Fe^{3+}, Cr^{3+}, Mn^{4+}).

Early work [8–10] established that the chromic ion enters the MgO lattice substitutionally on cation sites. Cr^{3+} was either found in a purely cubic environment or was observed [8–10] to occupy tetragonal (⟨1 0 0⟩ axis) and orthorhombic (⟨1 1 0⟩axis) sites; these latter defects are present in smaller numbers than the former. Because of the low concentration of other possible compensating agents, these defects were ascribed [8, 10] to ⟨100⟩ and ⟨110⟩ solute–vacancy dimers, respectively (Fig. 1). Imbusch *et al.* [11] studied the tetragonal centre by observing the changes in the luminescence spectrum produced by the application of uniaxial stresses, demonstrating conclusively the ⟨100⟩ axis of symmetry. The nature of the luminescence indicated a defect of odd symmetry, and the ⟨100⟩ dimer, $(Cr_{Mg}^{\cdot}–O–V_{Mg}'')'$, was suggested. These workers also reported lines which they attributed to the linear neutral ⟨100⟩ trimer analogous to the dimer, $(Cr_{Mg}^{\cdot}–O–V_{Mg}''–O–Cr_{Mg}^{\cdot})^{x}$.

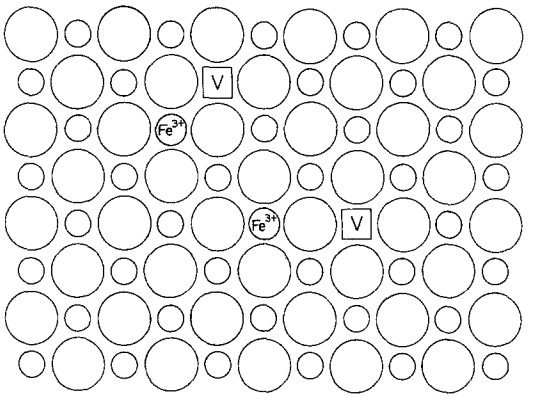

Figure 1 Two possible orientations of impurity–vacancy dimers in MgO (shown with Fe^{3+}). Trimers are the obvious linear extension of the dimers.

Glass [12] further investigated the luminescence of magnesia doped with 75 ppm chromium as a function of heat-treatment in the temperature range 400 to 900° C. The assignments of spectral lines to ⟨100⟩ dimers and trimers by previous workers [8–11] were adopted and, on the basis of semi-quantitative arguments, various weaker lines were attributed to a ⟨110⟩ dimer $(Cr_{Mg}^{\cdot}–V_{Mg}'')'$, and a non-linear trimer. By assuming that the concentration of a given defect was proportional to the intensity of the luminescence line, Glass [12] was able to analyse his data as a function of tem-

*Unless otherwise indicated, "vacancy" should be understood as "cation vacancy."

†Kroger–Vink notation for defects will be used throughout this paper. Readers unfamiliar with the conventions are referred to a general review such as that given by Kingery *et al.* [58], Ch. 4.

perature in terms of the mass-action equilibrium expressions for the various associates. The ⟨110⟩ dimer was found to be energetically more stable than its ⟨100⟩ counterpart (i.e. ΔE for the former is more negative). However, the pre-exponential factor of the ⟨110⟩ defect is more than two orders of magnitude less than that of the ⟨100⟩ defect, accounting for Glass' observation that the ⟨100⟩ associates are present in greater concentration than the ⟨110⟩. An examination of Figs 7 to 9 of [12] shows that, with the exception of the formation of the ⟨100⟩ trimer from the ⟨100⟩ dimer, the fit of the data to a simple mass-action defect model is not completely convincing. The effects of other aliovalent impurities* were not fully considered, but are certainly important (particularly at low Cr concentrations). The identities of the centres producing some of the weaker lines remain open to question, and in fact some very weak lines were not assigned. It is also curious, for example, that the ⟨110⟩ trimer does not appear; one would expect, too, that larger clusters might form at the low temperatures used. Anomalous behaviour of the luminescence spectrum above 900° C remains to be explained. Thus, although by no means definitive, Glass's [12] study is nevertheless an important attempt to account for the behaviour of a variety of defect centres in terms of mass-action relationships.

In a parallel study of Cr^{3+} in MgO, Wertz and Auzins [13] studied the ESR spectrum of Cr^{3+} and also found two sets of centres having tetragonal and orthorhombic symmetry. One set, termed T and R, was attributed to the expected dimers having ⟨100⟩ and ⟨110⟩ orientations. The second set, termed T′ and R′, was associated with linear neutral trimers having ⟨100⟩ and ⟨110⟩ axes, respectively, and involving a second trivalent impurity, perhaps Al^{3+}. Henderson and Hall [7] also studied the T′ centre, but make no mention of defects of orthorhombic symmetry. The temperature behaviour of the ESR spectrum observed by Wertz and Auzins [13] suggests that larger clusters of solute ions may form at temperatures below about 700° C† over a period of several days. Assuming an effective diffusion coefficient of 10^{-17} to 10^{-18} cm^2 sec^{-1} and a diffusion distance of 100 Å ([Cr] ≈ 100 ppm), this is not unreasonable. Magnetic susceptibility measurements [14] on polycrystalline samples of magnesia containing 0.9% Fe^{3+} have indicated that clusters containing as few as six solute ions can form, even in specimens quenched from 1400° C.

The Mn^{4+} ion has been studied by a number of workers [6, 7, 15] and, like Cr^{3+}, it enters the lattice substitutionally. Only a tetragonal centre has been reported in addition to purely cubic Mn^{4+} and this is attributed to the neutral ⟨100⟩ dimer; but Henderson and Hall [7] suggest that a substitutional monovalent ion might be the compensating agent.

Iron also enters the magnesia lattice substitutionally [16, 17] and usually occurs as Fe^{2+} or Fe^{3+}, although Fe^{+} may be produced upon irradiation [18]. The relative amounts of ferrous and ferric iron may be changed by heat-treatment [16]. Henderson *et al.* [19] studied the EPR spectrum of the ferric ion in magnesia and observed a tetragonal centre which they identified as the ⟨100⟩ dimer. A weaker set of lines was tentatively assigned to the ⟨110⟩ dimer.

Unruh *et al.* [20] studied the ESR and ENDOR (electron nuclear double resonance) spectra of the trapped hole V^- centre previously investigated by Wertz and co-workers [18, 21, 22]. On the basis of the ENDOR spectrum, they suggest that the centre is, in fact, an aluminium–vacancy associate having a ⟨100⟩ axis of symmetry. The half-life of the centres (10 h at room temperature) is in accordance with this assignment, as are the dramatic increases in both ESR and ENDOR signals with the aluminium content of the crystals. It is important to note that these workers infer the presence of a compensating vacancy both from impurity spectra and from direct observations on a vacancy centre. This is in contrast to previous studies which infer the presence of the vacancy on the basis of observations only on the impurity.

This survey indicates the narrow limits to our knowledge of the structure and stability of impurity defects in MgO; the data on impurity migration is even more restricted. Thus tracer diffusion coefficients of Al^{3+} and Fe^{3+} have not been measured in magnesia, but experiments with other cation impurities with valences of + 2, + 3 and + 4 are consistent in yielding small (10^{-4} cm^2 sec^{-1}) pre-exponentials and modest (2 eV) energies of activation [23]. This information, as Wuensch [23] points out in his general review, indicates that the tracer diffusion of cation impurities is extrinsic

*Fe, 200 ppm; Al, 50 ppm; Mn, 100 ppm; Si, 50 ppm.
†The Cr concentration of the sample is not given.

and the observed activation energy is that for ionic motion. Interdiffusion studies in the MgO–$MgAl_2O_4$ system [24] yielded an activation energy for self-diffusion of Al^{3+} in MgO of 3.3 eV. Using luminescence techniques, Glass and Searle [25] studied the migration of the $(Cr_{Mg}^{\cdot}-O-V_{Mg}'')'$ associate and deduced an activation energy of 1.73 eV.* More recently, Weber *et al.* [26] found an activation energy of 2.8 eV for chromium self-diffusion in single-crystal specimens containing a total of 250 ppm aliovalent impurity. Diffusion in samples doped with chromium, however, showed activation energies of only 1.2 eV [26]. The origin of this discrepancy is not clear, and the possibility of such concentration-dependent effects makes the interpretation of experimental activation energies difficult.

We can now usefully summarize our survey, which though brief and selective, is also representative. Almost all of the work supports a few basic generalizations: (1) a number of different cation impurities (Fe^{3+}, Al^{3+}, Cr^{3+}, Mn^{4+}) behave in a similar way in magnesia, forming analogous associates; (2) available data are consistent with a variety of aliovalent impurity–vacancy associates, including dimers and trimers oriented along either a ⟨110⟩ or ⟨100⟩ axis; (3) defects having a ⟨100⟩ axis of symmetry are observed to predominate over those with a ⟨110⟩ axis, so much so that evidence for orthorhombic (⟨110⟩) centres may be termed sketchy; (4) larger, more complicated clusters may have a substantial effect on the defect equilibria at low temperatures; (5) activation energies of motion for cation impurities are, with few exceptions, of the order of 2 eV. Despite this general broad consensus, it is fair to state that a detailed experimental knowledge of solute behaviour at the microscopic level in magnesia remains limited and, in some respects, confused. This situation makes the use of lattice calculations desirable both for a qualitative clarification of what defect configurations are stable as well as for a quantitative determination of their energies of formation.

3. Calculations and lattice models

3.1. Calculations

The Harwell Automatic Defect Evaluation System (HADES) is a versatile and efficient program which uses the shell model [27, 28] to evaluate defect energies in ionic solids; we discuss details of the lattice models in the next sections. Details of the method of calculation are found elsewhere [29–32] and we give only an abbreviated outline of the basic features of the program, sufficient for an understanding of the results presented here.

Conceptually, the HADES scheme is straightforward. The lattice displacements, dipoles and energies are evaluated exactly and explicitly in the region immediately surrounding the defect (region I), since this is the region in which most of the distortion occurs. Far from the defect (region II) only the net monopole field due to the defect is important in determining the displacements and dipoles; this contribution to the energy of the defect is thus a monopole–dipole term which has the form $\frac{1}{2}QV$, where Q is the net defect charge and V is the potential at the defect due to the induced lattice polarization.† To minimize errors that come from applying different techniques in the two regions, a "buffer" zone, IIa, is provided to include explicit interactions between region I and the inner part of region II. The total energy is then the sum of these three energies. This approach yields results which are equivalent to those obtained using less efficient techniques [2].

3.2. Lattice models

The shell model used in these calculations provides a generally satisfactory description of the elastic and dielectric properties of ionic solids and is adequate for defect calculations. In this model, each ion is represented by a charged core and shell which are coupled harmonically; the displacement of core and shell represents the ionic polarization. The repulsive overlap interaction between closed-shell ions acts between the ion shells and there is, in consequence, a coupling between the overlap interactions and ionic polarization. This coupling is necessary to account for the observed dielectric properties of the crystal. It is omitted from simpler descriptions of ionic crystals such as the polarizable point-ion model.

The magnitudes of the various interactions in the shell model are conveniently fitted to bulk

*Their analysis is too simplistic, however, since at least two types of jumps are required for the motion of the dimer.

†Catlow *et al.* [2] found that the inclusion of the elastic displacement field has a negligible effect on the calculated energies of vacancy formation. Consequently, it was ignored here. Elastic displacements are of major importance, however, in the calculation of dislocation energies [33, 34].

lattice properties; Catlow *et al.* [2] have developed two shell models for MgO and calculated vacancy formation energies. In these models, the total ion charges (the sum of core and shell charges) were set to + 2 and − 2. The anion core–shell coupling constant and the magnitude of the anion shell charge were determined by fitting to the dielectric constants ϵ_0 and ϵ_∞ and the transverse optic frequency ω_T; the cations are unpolarizable.

The cation–anion overlap repulsion was represented by a Born–Mayer potential $\Phi^R_{+-}(r) = A_{+-}\exp(-r/\rho_{+-})$ where the parameters A_{+-} and ρ_{+-} were fitted to elastic data for MgO and the lattice stability condition; this potnetial acted only between nearest-neighbour ions. The anion–anion interactions, however, are essentially attractive. Even if a conventional estimate of the oxygen–oxygen van der Waals interaction is added to a Born–Mayer overlap potential and if this is then fitted to crystal data, the Born-Mayer term is still attractive. This phenomenon is discussed and considered in detail in recent papers [36, 37] that propose more sophisticated potentials for ionic crystals. The simplest acceptable solution to this difficulty, however, is to supply a calculated estimate of the repulsive part of the second-neighbour interaction and then fit the van der Waals parameter C_{--} in the complete anion–anion potential $V(r) = A_{--}\exp(-r/\rho_{--}) - C_{--}/r^6$. However, O^{-2} is not bound and Catlow *et al.* [2] were obliged to use a calculated O^-–O^- overlap potential in place of the actual interaction between O^{-2} ions; this is probably a reasonable approximation at close interionic separations. This composite anion–anion potential then acts only between nearest pairs of oxygen ions. Cation–cation interactions are very small and they were omitted from the model.

The short-range potentials thus incorporate three unknown parameters, A_{+-}, ρ_{+-} and C_{--}; these were fitted to elastic data and the lattice stability condition for MgO. Because the shell model is not a complete description of MgO, this fitting procedure is not uniquely defined. The shell model, with only central pair potentials, can represent a crystal only with $C_{12} = C_{44}$; data for MgO do not satisfy this Cauchy condition. A harmonic energy due to an isotropic distortion of the anion shell has been used to provide *a priori* a calculated difference between C_{12} and C_{44}. The effect on calculated defect energies is small [2, 38], and the "breathing" terms are perhaps more important in the description of lattice dynamics [39] and the calculation of dislocation phenomena [33, 34]. The breathing terms do not influence the values of the shear moduli C_{44} and $C_{11}-C_{12}$; the preferred model of Catlow *et al.* [2] was, therefore, fitted to these data and to the lattice-stability condition.

TABLE I MgO model parameters (model 1)

(a) Repulsive potential

$$\Phi^R_{ij} = A_{ij}\exp(-r/\rho_{ij})$$

Interaction	A(eV)	ρ(Å^{-1})
Mg^{2+}–O^{2-}	1 152.0	0.3065
O^{2-}–O^{2-}	22 760.0	0.1490

(b) Van der Waals potential

$$\Phi^{vdW}_{ij} = -c_{ij}/|r_{ij}|^6$$

Interaction	c
O^{2-}–O^{2-}	28.96

The model of MgO used in this work is the preferred model of Catlow *et al.* [2]. The potential parameters are collected in Table I; the values of the crystal data calculated $(-r/\rho_{+-})$ model are compared with experiment in Table II. There is a good representation of the dielectric properties of the crystal, and recent experience indicates that this is essential for calculating reliable energies of charged defects in ionic crystals. Catlow *et al.* [2] also showed that their results for vacancy energies in MgO are robust against significant changes in the model. The use of an alternative model, with the same potential parameters fitted to C_{11} and C_{12} separately, produced some variation in the separate formation energies of cation and anion vacancies, but the physically significant Schottky energy was almost unchanged. This suggests that relative defect energies* are largely independent of the crystal model used as long as it describes the materials properties at least approximately.

We thus believe that the physically significant defect energies considered in this paper are not dependent on the limitations of the lattice model.

*Absolute energies of defect formation are the energy changes when defect constituents which are added or removed from the perfect crystal are brought up from or are taken to the zero of energy at infinity. Relative energies are differences between absolute energies. Thus, the binding energy of a complex associate with respect to its separated constituents is a relative energy.

TABLE II Crystal constants

Quantity	Calculated	Experimental
E_c (cohesive energy)	−40.87 eV	−40.06
ϵ_∞	2.96	2.95
ϵ_0	9.86	9.65 -- 9.86
C_{11}	3.555×10^{12} dyn cm^{-2}	2.892×10^{12} dyn cm^{-2}
C_{12}	1.547×10^{12} dyn cm^{-2}	8.80×10^{11} dyn cm^{-2}
C_{44}	1.547×10^{12} dyn cm^{-2}	1.546×10^{12} dyn cm^{-2}
$C_{11} - C_{12}$	2.008×10^{12} dyn cm^{-2}	2.012×10^{12} dyn cm^{-2}
a_0 (lattice constant)	–	2.106 Å

They are, however, much more influenced by choice of the potentials describing the impurity lattice interaction.

3.3. The impurity lattice interaction

A problem of major importance is determination of the proper cation solute–oxygen repulsive interactions in the MgO host lattice. As will be seen in the following section, these terms have a significant effect on the calculated binding energies for the associates of interest. Since our observation is that the anion–cation repulsive interaction is dominant, a reasonable approach is to use potentials which adequately describe the pure solute oxide. Thus, the Al^{3+}–O^{2-} potential used was taken from the recent shell model calculations of Dienes *et al.* [40] for Al_2O_3. This set of parameters, calculated using a Wedepohl [41] technique, describes the bulk modulus and cohesive energy of alumina fairly well within the context of a crystal model similar to that of HADES. The Dienes potential, however, does not fit the simple Born–Mayer form over a wide range of separations (Fig. 2). Since HADES has no provision for such non-linearity, a single approximate potential was obtained for separations in the range 1.5 to 2.54 Å.

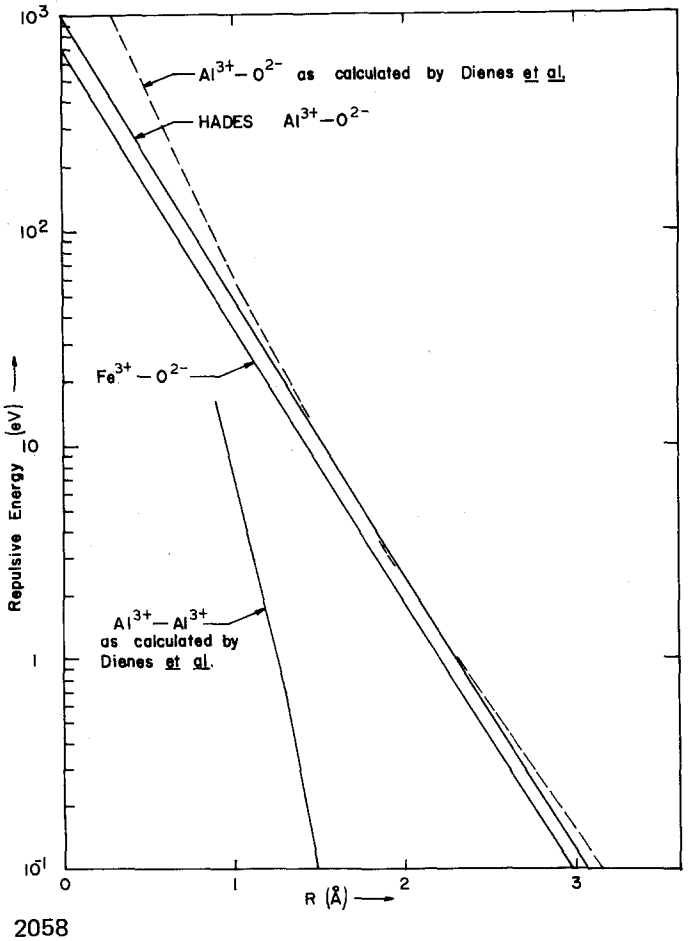

Figure 2 Plot of the Born–Mayer potentials for Al^{3+}–O^{2-} and Fe^{3+}–O^{2-} interactions. Potentials of Dienes *et al.* [40] provided for comparison.

TABLE III Born–Mayer parameters for impurity–oxygen interactions

Interaction	A(eV)	$\rho(\text{Å}^{-1})$
Fe^{3+}–O^{2-}	702.29	0.3362
Fe^{2+}–O^{2-}	745.30	0.3362
Al^{3+}–O^{2-}	1000.00	0.3325
Ion	Radius (Å)	
Fe^{2+}	0.82	
Fe^{3+}	0.7–0.8	
Al^{3+}	0.57	

The parameters for this potential are collected in Table III, and the resultant straight line is indicated in Fig. 2. Since Al^{3+} and Mg^{2+} have the same electronic state and are similar in size, one would expect their interactions with O^{2-} to be quite similar, so the values given in Table III are reasonable. For their investigation of wüstite, Catlow and Fender [42] derived a potential for Fe^{2+}–O^{2-}. From this they obtained a potential for Fe^{3+}–O^{2-} interactions using a scaling procedure based on the ionic radii. The coefficient, ρ_{+-}, is thus taken to be the same for both Fe^{2+} and Fe^{3+}, but the pre-exponential of the latter is scaled by the factor $\exp((r_{Fe^{3+}} - r_{Fe^{2+}})/\rho_{+-})$ where r is the appropriate ionic radius. Of course, such a method depends rather critically on the radii used, and it is not clear what radii are most appropriate, since the values change in different environments. Catlow and Fender [42] took $r_{Fe^{3+}} = 0.80$ Å, only slightly less than that for Fe^{2+} (0.82 Å), because this value takes "account of the absence of ligand field stabilization energies for the d^5 ferric ion" [42].* These potentials, which were used here, are given in Table III and that for Fe^{3+}–O^{2-} is plotted in Fig. 2. A comparison of Φ^R for Fe^{3+} and Al^{3+} in Fig. 2 indicates that, if these potentials are at least approximately correct, the concept of the repulsion arising from the overlap of charge clouds having the ionic radius is of questionable value. At a given separation, the energy of the smaller ion (Al^{3+}, $r \approx 0.6$ Å) is larger. Although differences in electronic configuration must be considered† and some available data indicate that this relative placement is correct, comparison with calculations indicates that this Fe^{3+}–O^{2-} interaction is too weak. Because of the *ad hoc* nature of its derivation, the ferric ion potential must be considered uncertain.

TABLE IV Simple impurity defect energies

Process	Absolute energy (eV)
$Mg^x_{Mg} + Fe^{2+}_\infty \rightarrow Mg^{2+}_\infty + Fe^x_{Mg}$	1.39
$Mg^x_{Mg} + Fe^{3+}_\infty \rightarrow Mg^{2+}_\infty + Fe^{\cdot}_{Mg}$	−29.67
$Mg^x_{Mg} + Al^{3+}_\infty \rightarrow Mg^{2+}_\infty + Al^{\cdot}_{Mg}$	−24.98
$-Fe^{2+}_\infty \rightarrow Fe^{\cdot\cdot}_i$	−10.17
$Fe^{3+}_\infty \rightarrow Fe^{\cdot\cdot\cdot}_i$	−42.29
$Al^{3+}_\infty \rightarrow Al^{\cdot\cdot\cdot}_i$	−33.84
Process	**Relative energy (eV)**
$Fe^x_{Mg} \rightarrow Fe^{\cdot\cdot}_i + V''_{Mg}$	12.27
$Fe^{\cdot}_{Mg} \rightarrow Fe^{\cdot\cdot\cdot}_i + V''_{Mg}$	11.20
$Al^{\cdot}_{Mg} \rightarrow Al^{\cdot\cdot\cdot}_i + V''_{Mg}$	14.97

Even the relative energies of solute associates were found to depend somewhat on the solute–oxygen repulsive interactions. Hence within this range of variation the calculated values, as they pertain to the Fe^{3+}, and Fe^{2+} ions, should be viewed with some caution. The variations are not great, however, and important trends are unaffected by reasonable variations in repulsive parameters. Insofar as the parameters used here represent a realistic range of solute properties, it is useful to view the results as representing changes in the crystal behaviour as the properties of the solute ion are varied.

4. Results and discussion

The calculations fall into four categories:‡ simple impurity defects, simple impurity vacancy associates, complex impurity associates and energies of ionic motion.

4.1. Simple impurity defects

The energies of substitutional impurity ions in the model MgO lattice are given in Table IV. These values correspond to the energy required to remove a magnesium ion to infinity and bring the indicated cation up from infinity to replace it.§ They

*The ionic radii for iron used by Catlow and Fender [42] were derived by Dickens *et al.* [43]. Corrections were applied to the Fe^{3+} radius in Fe_2O_3 (0.67 Å) to obtain an estimate of the effective radius of this ion in a rocksalt crystal environment (0.80 Å). This range of values is indicated in Table III. Shannon and Prewitt [44] discuss the derivation and interpretation of ionic radii in detail.

†The localized d states of iron ions may produce non-central or asymmetric repulsive forces. Crystal field effects may also affect interactions with the oxygen ion. These details are ignored here, an admitted deficiency.

‡A fifth, intrinsic defect, in included as Appendix 3.

§The effects of a free surface upon the substitutional energies of solutes in ionic crystals have been considered in recent calculations. See [54] and [55].

are thus absolute energies in the sense described earlier, and are sensitive to the parameters of the impurity–oxygen repulsive interaction.

The energy of solution for the process:

$$Al_2O_3(s) \xrightarrow{MgO} 2Al^{\cdot}_{Mg} + V''_{Mg} + 3O^{x}_{0} \qquad (1)$$

may be estimated as:

$$\Delta E_s = 2E_{Al^{\cdot}_{Mg}} + E_{V''_{Mg}} + 3E_c^{MgO} - E_c^{Al_2O_3}. \qquad (2)$$

When compared with similar estimates derived from phase diagram data (Appendix 1), such a calculated heat of solution provides a useful check on the validity of the solute parameters. It is important to notice, however, that ΔE_s is the difference between rather large numbers so that high accuracy, or at least great consistency, is required in the calculation of each energy if a reasonable result is to be obtained. $E_{Al^{\cdot}_{Mg}}$, $E_{V''_{Mg}}$ and E_c^{MgO} are all derived from HADES calculations so that it will be assumed that the sum $2E_{Al^{\cdot}_{Mg}} + E_{V''_{Mg}} + 3E_c^{MgO}$ is correct to within the error in the cohesive energy term, $3E_c^{MgO}$. Estimating this error is difficult because the cohesive energy cannot be measured directly, but must be calculated from thermodynamic data, as in the Born–Haber cycle [45–47]. E_c is particularly troublesome to obtain for oxides because the free O^{2-} ion is unstable and its energy of formation from the neutral oxygen atom cannot be determined independently. Estimates of this electron affinity, $E(O^{2-})$, are derived from the calculated cohesive energies of oxides (presumed to be ionic) and the various other data in the Born–Haber cycle. There is a considerable variation in the resulting affinities, and the major source error in "experimental" (i.e. Born–Haber) cohesive energies is the uncertainty in $E(O^{2-})$ [45–48]. Taking this uncertainty to be ± 0.5 to 0.7 eV [45, 46], the uncertainty in $3E_c^{MgO}$ is ± 1.5 to 2.1 eV. Sherman [45] gives a value for $E_c^{Al_2O_3}$ of −157.0 eV*, for which one can estimate an error of ± 1.5 to 2.1 eV. Evaluating ΔE_s, and using these estimated uncertainties, one obtains $\Delta E_s = 8.2 \pm 2.3$ eV. This is large, but is compatible with heats of solution (4.1 to 8.4 eV) derived from a simple thermodynamic analysis of solid solubility data discussed in Appendix 1. Although not conclusive, since the probable errors are large, this agreement demonstrates that the parameters used may adequately and realistically describe the behaviour of the aluminium ion in magnesia. It has already been noted that, because the magnesium and aluminium ions are isoelectronic and have ionic radii which are not vastly different†, one would expect their repulsive potentials to be similar. On the basis of such a comparison (Tables I and III), the potential for Al^{3+} appears reasonable.

In contrast, an analogous calculation for Fe_2O_3 yields to a solution, ΔE_s, of -2.9 ± 3 eV. The cohesive energy of Fe_2O_3, −155.2 eV, is derived in [35] from a Born–Haber cycle using oxygen electron affinity data given by Waddington [46]. Even within an error margin of 100%, this result is not compatible with the limited solubility of Fe_2O_3 in magnesia. On this basis alone a positive heat of solution is to be anticipated and the analysis given in Appendix 1 indicates a value between 6.0 and 3.5 eV. Since the errors in the cohesive energy (± 2 eV) are probably not large enough to account for the negative value calculated, it seems that some of the difficulty lies in the repulsive potential used for Fe^{3+}. The potential is apparently too weak in that it permits excessive relaxation around the impurity cation yielding too negative a substitutional energy. Changes of two or three electron volts in the substitutional energy would produce agreement between the theoretical and derived energies of solution. Such variations are certainly within a realistic range of impurity parameters. Thus, we believe that the potential used for iron is incorrect, but not grossly so. Together with the potential for aluminium, it brackets a region of plausible impurity behaviour.

Interstitial energies for Fe^{2+}, Fe^{3+} and Al^{3+} are also given in Table IV. The lower values for iron result from the repulsive potential parameters used. Nonetheless, it seems that energies to be expected are large, as for intrinsic interstitials (Appendix 3).

4.2. Simple associates

Two configurations of impurity–vacancy dimers in MgO are shown in Fig. 1. In one case the impurity and vacancy are on nearest-neighbour cation sites and lie along a ⟨110⟩ axis. In the other, the two defects occupy next nearest cation sites, with an oxygen ion between them along a ⟨100⟩ axis. The calculated binding energies of these dimers,

*A Born–Haber calculation using more recent data gives $E_c^{Al_2O_3} = 159.0$ eV, which is within the error range suggested.
†$r_{Mg^{2+}} = 0.67$ to 0.72 Å, $r_{Al^{3+}} = 0.5$ to 0.6 Å.

TABLE V

Process	Energy (eV)
$Fe^{\cdot}_{Mg} + V''_{Mg} \rightarrow (Fe^{\cdot}_{Mg}-V''_{Mg})'$	− 0.85
$Fe^{\cdot}_{Mg} + V''_{Mg} \rightarrow (Fe^{\cdot}_{Mg}-O-V''_{Mg})'$	− 1.13
$2Fe^{\cdot}_{Mg} + V''_{Mg} \rightarrow (Fe^{\cdot}_{Mg}-V''_{Mg}-Fe^{\cdot}_{Mg})^{x}$	− 1.42
$2Fe^{\cdot}_{Mg} + V''_{Mg} \rightarrow (Fe^{\cdot}_{Mg}-O-V''_{Mg}-O-Fe^{\cdot}_{Mg})^{x}$	− 2.20
$Fe^{\cdot}_{Mg} + V''_{Mg} \rightarrow (Fe^{x}_{Mg}-V''_{Mg})''$	− 0.03 (~ 0.0)
$Al^{\cdot}_{Mg} + V''_{Mg} \rightarrow (Al^{\cdot}_{Mg}-V''_{Mg})'$	− 0.68
$Al^{\cdot}_{Mg} + V''_{Mg} \rightarrow (Al^{\cdot}_{Mg}-O-V''_{Mg})'$	− 0.86
$2Al^{\cdot}_{Mg} + V''_{Mg} \rightarrow (Al^{\cdot}_{Mg}-V''_{Mg}-Al^{\cdot}_{Mg})^{x}$	− 1.32
$2Al^{\cdot}_{Mg} + V''_{Mg} \rightarrow (Al^{\cdot}_{Mg}-O-V''_{Mg}-O-Al^{\cdot}_{Mg})'$	− 1.68

relative to the separated constituents, are given in Table V* and the displacements of the surrounding ion cores and shells in Fig. 3 and 4. The most striking feature of the results in Table V is the stability of the ⟨100⟩ relative to the ⟨110⟩ orientation. This effect seems to be independent of changes in the impurity–oxygen repulsion, since it is observed for both aluminium and iron. In contrast, a simple coulomb calculation of the expected binding energies for these dimers, which yields surprisingly good agreement for the divacancy (Appendix 3), indicates that, because of the closer proximity of the impurity and vacancy, the ⟨110⟩ orientation should be more stable. Examination of Fig. 4 shows that the central oxygen ion (labelled A) plays a key role in the stability of the ⟨100⟩ dimer. The core displacement and polarization (shell displacement) of this ion are 2 to 4 times greater than those of other oxygen ions around the associate. Fixing the oxygen-ion core decreases the binding energy of the ⟨100⟩ dimer by half and fixing the oxygen-ion shell decreases the binding energy to a fifth of its original value. Clearly, the juxtaposition of the "negatively charged" vacancy and the "positively charged" impurity on either side of the single central oxygen induces large relaxations which result in a large decrease in the energy, both from the coulomb interaction and the dipole field. Although the displacements and polarizations around the ⟨110⟩ dimer are large, there is no single source of a large perturbation.

The binding energies of the linear neutral trimers analogous to the dimers are also given in Table V, and the core displacements are shown in Fig. 5. Less symmetric trimer formations (combinations of ⟨100⟩ and ⟨110⟩ dimers) are possible, and were considered by Glass [12], but were not included in this study. From Fig. 5 and the binding energies of Table V, it is apparent that these simple trimers are essentially two dimers placed

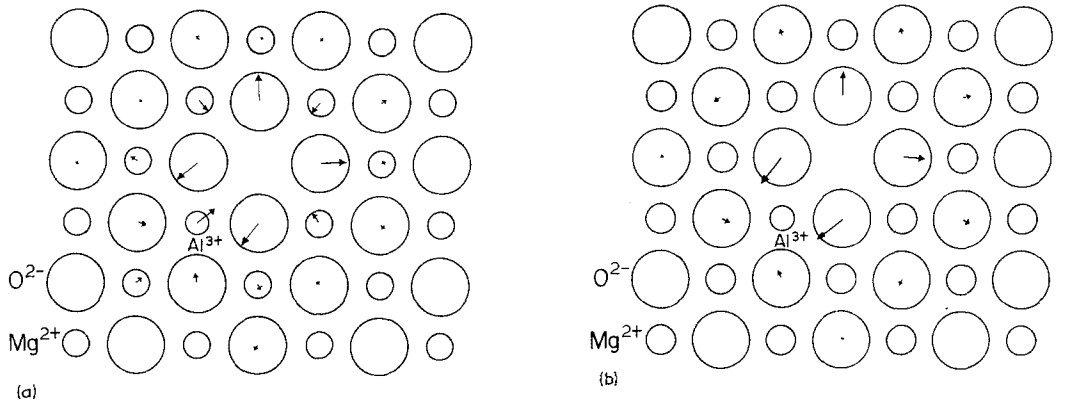

Figure 3 Displacements around a ⟨100⟩ dimer. (a) Ion core displacements (× 5). (b) Shell displacements (× 20).

*The rather large binding energies for associates containing "iron" are a result of the softness of the repulsive potential used for the iron impurity. Excessive relaxation around the substitutional ion permits the defect energy to become large and negative with the result that the associate binding energies are large.

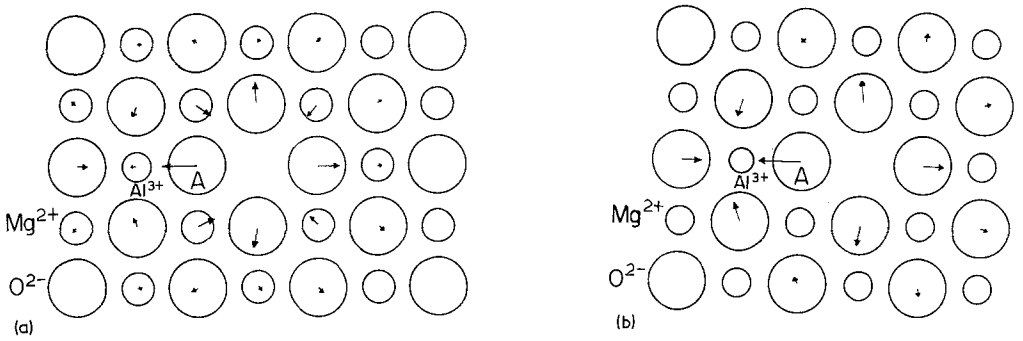

Figure 4 Displacements around a ⟨1 0 0⟩ dimer. (a) Ion core displacements (× 5). (b) Shell displacements (× 20).

end-to-end, sharing a common vacancy. Thus, the ⟨1 0 0⟩ trimers are considerably more stable than their ⟨1 1 0⟩ counterparts.

These results are contrary to the quantitative interpretation of Glass [12] for chromium-doped magnesia, but are consistent with his and others' observations that defects of ⟨1 0 0⟩ symmetry are present in greater quantity than those having ⟨1 1 0⟩ symmetry.

No significant binding energy was found between divalent substitutional iron and a cation vacancy in the ⟨1 1 0⟩ orientation. This is to be expected, since a divalent substitutional impurity has no effective charge relative to the lattice. The binding energy of the ⟨1 0 0⟩ ferrous dimer is likewise expected to be zero or small.

4.3. Complex solute–vacancy associates

In view of the possible importance of clustering on physical properties and in the precipitation of magnesium aluminate (spinel) and magnesium ferrite from magnesia solid solution, the complex impurity–vacancy aggregates considered here were "spinel-like" in that all contained a basic structural unit consisting of a tetrahedrally co-ordinated interstitial cation surrounded by four cation vacancies. Because of the strong preference of aluminium for octahedral co-ordination, Mg^{2+} ions were placed in the interstitial positions of aluminium aggregates. Magnesium ferrite, in contrast, is nominally an inverse spinel,* so in the case of iron impurities the ferric ion was placed at interstitial sites. To avoid large polarization energies in region II and to provide a realistic matching of ionic and shell displacements across the boundary between regions I and II, it is necessary to work with clusters which are at least approximately neutral. Compensating substitutional impurities (Al^{3+}, Fe^{3+}) were thus placed in symmetrical positions about the cluster to bring its net charge within the range $-2e$ to $+2e$. The symmetry necessary for the efficient analysis of these large groupings,

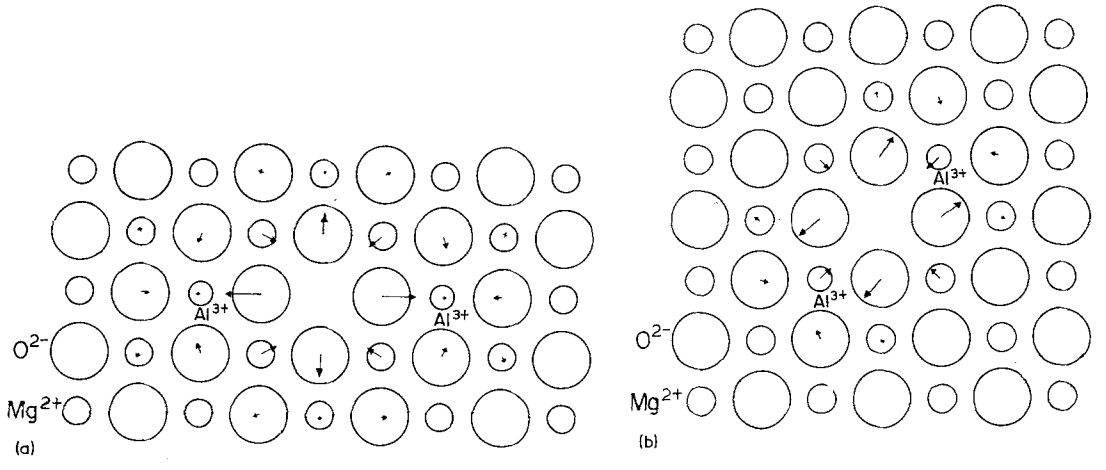

Figure 5 Ion core displacements (× 5) around ⟨1 0 0⟩ and ⟨1 1 0⟩ trimers. (a) ⟨1 0 0⟩ trimer. (b) ⟨1 0 0⟩ trimer.

*For a discussion of spinel structures see, for example, Kingery *et al.* [58] Ch. 2.

TABLE VI

Process	Energy (eV)	Remarks
$2Fe^{\cdot}_{Mg} + V''_{Mg} \rightarrow (Fe^{\cdot}_{Mg}-O-V''_{Mg}-O-Fe^{\cdot}_{Mg})^{x}$	− 2.20	⟨100⟩ trimer, − 2.20 per net vacancy
$6Fe^{\cdot}_{Mg} + 3V''_{Mg} \rightarrow (4-1-Fe^{3+})^{x}$	− 6.08*	− 2.03 eV per net vacancy
$8Fe^{\cdot}_{Mg} + 4V''_{Mg} \rightarrow (6-2-Fe^{3+})^{x}$	− 10.48	− 2.62 eV per net vacancy
$22Fe^{\cdot}_{Mg} + 11V''_{Mg} \rightarrow (16-5-Fe^{3+})^{x}$	− 33.18*	− 3.02 eV per net vacancy
$22Fe^{\cdot}_{Mg} + 11V''_{Mg} + 5Mg^{x}_{Mg} \rightarrow (24-5-Fe^{3+})^{x}$	− 27.24*	− 2.48 eV per net vacancy
$2Al^{\cdot}_{Mg} + V''_{Mg} \rightarrow (Al^{\cdot}_{Mg}-O-V''_{Mg}-O-Al^{\cdot}_{Mg})^{x}$	− 1.68	⟨100⟩ trimer − 1.68 eV per net vacancy
$6Al^{\cdot}_{Mg} + 3V''_{Mg} + Mg^{x}_{Mg} \rightarrow (4-1-Al^{3+})^{x}$	− 4.77*	− 1.59 eV per net vacancy
$8Al^{\cdot}_{Mg} + 4V''_{Mg} + 2Mg^{x}_{Mg} \rightarrow (6-2-Al^{3+})^{x}$	− 6.17*	− 1.54 eV per net vacancy
$8Al^{\cdot}_{Mg} + 4V''_{Mg} + 2Mg^{x}_{Mg} \rightarrow (8-2-Al^{3+})^{x}$	− 8.93	− 2.23 eV per net vacancy
$22Al^{\cdot}_{Mg} + 11V''_{Mg} \rightarrow (16-5-Al^{3+})^{x}$	− 28.42*	− 2.58 eV per net vacancy
$22Al^{\cdot}_{Mg} + 11V''_{Mg} + 5Mg^{x}_{Mg} \rightarrow (24-5-Al^{3+})^{x}$	− 25.28*	− 2.30 eV per net vacancy
$22Al^{\cdot}_{Mg} + 11V''_{Mg} + 5Mg^{x}_{Mg} \rightarrow (24-5-Al^{3+}-a)^{x}$	− 28.23*	− 2.57 eV per net vacancy

* Approximate formation energy of the neutral defect.

however, precluded, in some cases, the explicit examination of the neutral cluster. In these instances, the energy of the neutral cluster was estimated simply by adding to (or subtracting from) the calculated energy, the energies of the isolated substitutional impurities necessary to yield a net charge of zero [42]. When the stability of the cluster relative to the separated defects is computed, these additional terms simply cancel out; thus, the binding energies reported for the neutral clusters do not, in most cases, include (or exclude) the explicit interactions of the additional ions with the remainder of the cluster. The energies reported are, strictly speaking, the binding energies or formation energies of the clusters having a net charge. Since one expects the addition of oppositely charged point defects to lower the energy, the energies calculated represent an upper bound (least negative) value for the energies of cluster formation. In any case, the binding energies obtained here give a clear indication of trends in the relative stability of large point defect aggregates.

Catlow and Fender [42] investigated spinel-like aggregates of point defects in FeO using HADES, and they found certain combinations of the basic tetrahedral unit to be particularly stable. Three of these configurations were used as starting points in this investigation: the "4-1", "6-2" and "16-5" cluster arrangements. In addition to these, a configuration corresponding to a normal spinel ("24-5") and a variant of the "6-2" ("8-2") were considered. The results of the calculations for these clusters are gathered in Table VI. Both the total energy of formation of the cluster from separated impurities and vacancies and the energy of formation per net vacancy are given. The energy per net vacancy (i.e. the total number of vacancies less the number of interstitials) provides a convenient means of comparing the stabilities of complex clusters with those of simpler associates, particularly dimers and trimers. Thus, if the energy per net vacancy is the same as or greater (less negative) than the energy of a neutral trimer, there would be no overall decrease in the crystal energy as a result of agglomeration of simpler groupings. In such a case, clusters would not form in significant numbers. If the energy per net vacancy is less than the energy of the neutral trimer, the larger clusters may become important equilibrium structures.

The structures and properties of the clusters are summarized in Table VII and Figs. 6 to 9. The simplest cluster, the "4-1", consists of a single tetrahedral unit with four compensating impurities in a symmetric arrangement off the four corners of the tetrahedron. A comparison of the binding energies per net vacancy given in Table VI with those given in Table V indicates that the "4-1" cluster is about as stable as the simple ⟨100⟩ trimers. It is worth emphasizing the profound effect of surrounding cation vacancies on the stability of cation interstitials. Whereas there is a rather large energy change opposing the formation of the simple interstitial defect (10 to 15 eV) (Appendix 3), the removal of four nearest cations renders the complex defect very stable.*

The "6-2" cluster, shown in Fig. 7a, consists of

*Admittedly, trivalent impurities have also been added. However, if one assumes their polarization and displacement fields simply superimpose, then the energy of formation of the interstital will be only slightly affected by the compensating ions, except for a coulomb interaction which is positive.

TABLE VII Complex associate structures

Associate	Centre of symmetry relative to f c c axes*	Location of compensating impurities relative to the centre of symmetry†	Net charge	Remarks
4–1–Fe^{3+} 4–1–Al^{3+}	$[\frac{1}{2}, \frac{1}{2}, \frac{1}{2}]$	$[-\frac{1}{2}, -\frac{1}{2}, 1\frac{1}{2}]$, $[-\frac{1}{2}, \frac{1}{2}, -1\frac{1}{2}]$ $[\frac{1}{2}, -\frac{1}{2}, -1\frac{1}{2}]$, $[\frac{1}{2}, \frac{1}{2}, 1\frac{1}{2}]$	−1	Single tetrahedral unit of four cation vacancies around an interstitial. Fe^{3+} interstitial for the iron cluster; Mg^{2+} interstitial for the aluminium.
6–2–Fe^{3+}	$[\frac{1}{2}, \frac{1}{2}, 0]$	$[\frac{1}{2}, \frac{1}{2}, 2]$, $[-\frac{1}{2}, -\frac{1}{2}, -2]$	0	Two edge-sharing
6–2–Al^{3+}		$[-\frac{1}{2}, -\frac{1}{2}, 2]$, $[\frac{1}{2}, \frac{1}{2}, -2]$ $[1\frac{1}{2}, 1\frac{1}{2}, 0]$, $[-1\frac{1}{2}, -1\frac{1}{2}, 0]$	−2	tetrahedral units
8–2–Al^{3+}	$[\frac{1}{2}, \frac{1}{2}, 0]$	$[\frac{1}{2}, \frac{1}{2}, 2]$, $[-\frac{1}{2}, -\frac{1}{2}, -2]$ $[-\frac{1}{2}, -\frac{1}{2}, 2]$, $[\frac{1}{2}, \frac{1}{2}, -2]$ $[-1\frac{1}{2}, \frac{1}{2}, 0]$, $[\frac{1}{2}, -1\frac{1}{2}, 0]$ $[-\frac{1}{2}, 1\frac{1}{2}, 0]$, $[1\frac{1}{2}, -\frac{1}{2}, 0]$	0	Alternate arrangement of compensating $Al_{Mg}^{\cdot}$ to give neutral defect, Mg^{2+}–Mg^{2+} repulstion included.
16–5–Fe^{3+}	$[-\frac{1}{2}, -\frac{1}{2}, -\frac{1}{2}]$	$[-2\frac{1}{2}, -\frac{1}{2}, \frac{1}{2}]$, $[-\frac{1}{2}, -2\frac{1}{2}, \frac{1}{2}]$, $[-2\frac{1}{2}, \frac{1}{2}, -\frac{1}{2}]$	−1	Inverse spinel structure.
16–5–Al^{3+}		$[\frac{1}{2}, -\frac{1}{2}, -2\frac{1}{2}]$, $[-\frac{1}{2}, \frac{1}{2}, -2\frac{1}{2}]$, $[\frac{1}{2}, -2\frac{1}{2}, -\frac{1}{2}]$ $[-\frac{1}{2}, 2\frac{1}{2}, -\frac{1}{2}]$, $[2\frac{1}{2}, -\frac{1}{2}, -\frac{1}{2}]$, $[\frac{1}{2}, 2\frac{1}{2}, \frac{1}{2}]$ $[2\frac{1}{2}, \frac{1}{2}, \frac{1}{2}]$, $[\frac{1}{2}, \frac{1}{2}, 2\frac{1}{2}]$, $[\frac{1}{2}, -\frac{1}{2}, 2\frac{1}{2}]$ $[1\frac{1}{2}, 1\frac{1}{2}, -1\frac{1}{2}]$, $[1\frac{1}{2}, -1\frac{1}{2}, 1\frac{1}{2}]$, $[-1\frac{1}{2}, 1\frac{1}{2}, 1\frac{1}{2}]$ $[-1\frac{1}{2}, -1\frac{1}{2}, -1\frac{1}{2}]$	−1	Corner-sharing tetrahedral arrangement of five tetrahedral units; Fe^{3+} and Al^{3+} interstitials
24–5–Fe^{3+}	$[-\frac{1}{2}, -\frac{1}{2}, -\frac{1}{2}]$	$[\frac{1}{2}, 2\frac{1}{2}, \frac{1}{2}]$, $[-\frac{1}{2}, -\frac{1}{2}, 2\frac{1}{2}]$ $[\frac{1}{2}, \frac{1}{2}, 2\frac{1}{2}]$	+2	Normal spinel structure.
24–5–Al^{3+}		$[\frac{1}{2}, -\frac{1}{2}, 1\frac{1}{2}]$, $[-\frac{1}{2}, \frac{1}{2}, 1\frac{1}{2}]$ $[\frac{1}{2}, 1\frac{1}{2}, -\frac{1}{2}]$, $[1\frac{1}{2}, -\frac{1}{2}, \frac{1}{2}]$, $[-\frac{1}{2}, 1\frac{1}{2}, \frac{1}{2}]$ $[1\frac{1}{2}, \frac{1}{2}, -\frac{1}{2}]$, $[-1\frac{1}{2}, -\frac{1}{2}, -\frac{1}{2}]$, $[\frac{1}{2}, -1\frac{1}{2}, \frac{1}{2}]$, $[-1\frac{1}{2}, \frac{1}{2}, \frac{1}{2}]$ $[-\frac{1}{2}, -1\frac{1}{2}, -\frac{1}{2}]$, $[\frac{1}{2}, \frac{1}{2}, -1\frac{1}{2}]$ $[-\frac{1}{2}, -\frac{1}{2}, -1\frac{1}{2}]$, $[-\frac{1}{2}, \frac{1}{2}, -2\frac{1}{2}]$ $[\frac{1}{2}, -\frac{1}{2}, -2\frac{1}{2}]$, $[-\frac{1}{2}, -2\frac{1}{2}, \frac{1}{2}]$, $[-2\frac{1}{2}, \frac{1}{2}, -\frac{1}{2}]$, $[\frac{1}{2}, -2\frac{1}{2}, -\frac{1}{2}]$ $[-2\frac{1}{2}, -\frac{1}{2}, \frac{1}{2}]$, $[2\frac{1}{2}, \frac{1}{2}, \frac{1}{2}]$, $[-\frac{1}{2}, 2\frac{1}{2}, -\frac{1}{2}]$, $[2\frac{1}{2}, -\frac{1}{2}, -\frac{1}{2}]$	+2	Corner-sharing tetrahedral arrangement of five tetrahedral units; Mg^{2+} interstitials
24–5–Al^{3+}–a	$[-\frac{1}{2}, -\frac{1}{2}, -\frac{1}{2}]$	As above with all co-ordinates containing $\pm\frac{1}{2}$, $\pm\frac{1}{2}$, and $\pm 2\frac{1}{2}$ replaced with: $[1\frac{1}{2}, 1\frac{1}{2}, 2\frac{1}{2}]$, $[1\frac{1}{2}, 2\frac{1}{2}, 1\frac{1}{2}]$ $[2\frac{1}{2}, 1\frac{1}{2}, 1\frac{1}{2}]$, $[-2\frac{1}{2}, -1\frac{1}{2}, 1\frac{1}{2}]$, $[-1\frac{1}{2}, -2\frac{1}{2}, 1\frac{1}{2}]$ $[-1\frac{1}{2}, -1\frac{1}{2}, 2\frac{1}{2}]$, $[-2\frac{1}{2}, 1\frac{1}{2}, -1\frac{1}{2}]$ $[-1\frac{1}{2}, 2\frac{1}{2}, -1\frac{1}{2}]$ $[-1\frac{1}{2}, 1\frac{1}{2}, -2\frac{1}{2}]$, $[1\frac{1}{2}, -1\frac{1}{2}, -2\frac{1}{2}]$ $[1\frac{1}{2}, -2\frac{1}{2}, -1\frac{1}{2}]$ $[2\frac{1}{2}, -1\frac{1}{2}, -1\frac{1}{2}]$	+2	Alternate arrangement of compensating cation impurities

* Centred on a cation. Units of a_0, the anion–cation distance.

† Units of a_0.

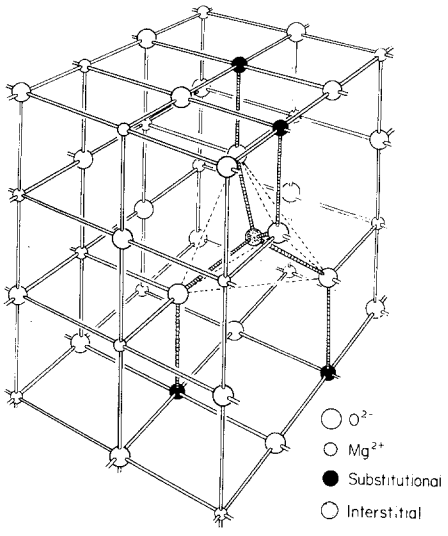

Figure 6 The 4-1 cluster.

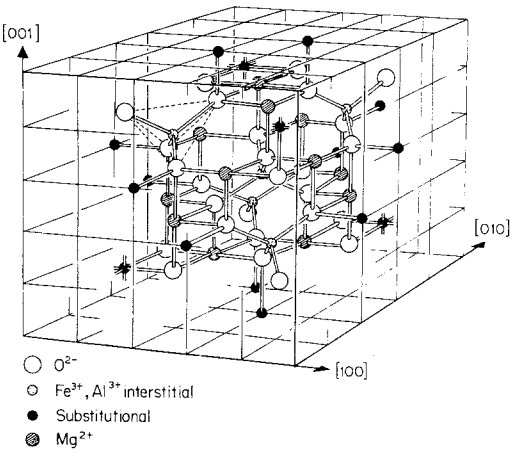

Figure 8 The 16-5 cluster.

two edge-sharing tetrahedral units with six symmetrically placed compensating impurities. This arrangement yields a net charge of zero for Fe^{3+} interstitials, but has a net charge of -2 for Mg^{2+} interstitials. An alternative configuration of eight substitutional impurities produces a neutral defect in this latter case (the "8-2" cluster, Fig. 7b). As suggested earlier, the explicit consideration of the neutral cluster gives a more negative value of the formation energy relative to a similar defect having a net charge, although the rearrangement of the impurities may play a role. In any case, the neutral configurations of these edge-sharing clusters are more stable than ⟨100⟩ trimers by about 0.4 to 0.5 eV in the cases of both Fe^{3+} and Al^{3+}.

The largest aggregates investigated model a substantial portion of the spinel unit cell, and consist of five corner-sharing tetrahedral units themselves arranged in tetrahedral symmetry. In the "16-5" configuration (Fig. 8) the trivalent octahedral ions are placed at the positions they would occupy in an ordered inverse spinel lattice. The "24-5" cluster, in contrast, mimics a normal spinel (Fig. 9). These large spinel-like aggregates are uniformly the most (energetically) stable defects considered. In the case of iron, the calculation shows the inverse ("16-5") structure to be more stable than the normal ("24-5") arrangement. Although this is satisfying, the same result is obtained in the case of Al^{3+} impurities, which is curious considering the strong preference for octahedral co-ordination shown by aluminium in $MgAl_2O_4$. Such a discrepancy may be a physical effect due to the fact that the cluster is surrounded by the MgO rather than the spinel lattice, but it could also be an artifact of the interionic potential model used. This anomaly is yet to be resolved, but calculations of site preference energies in the spinel lattice may prove useful in this regard.

The energy of the aluminium "24-5" cluster is

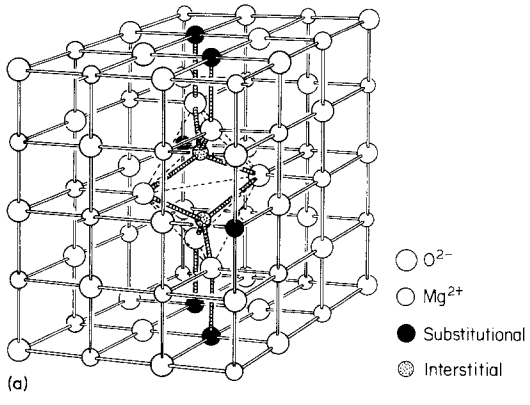

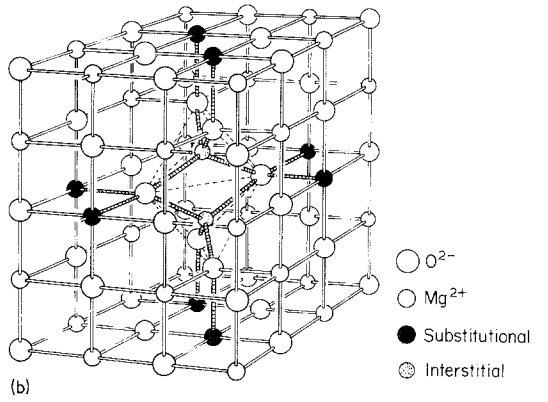

Figure 7(a) The 6-2 cluster. (b) The 8-2 cluster.

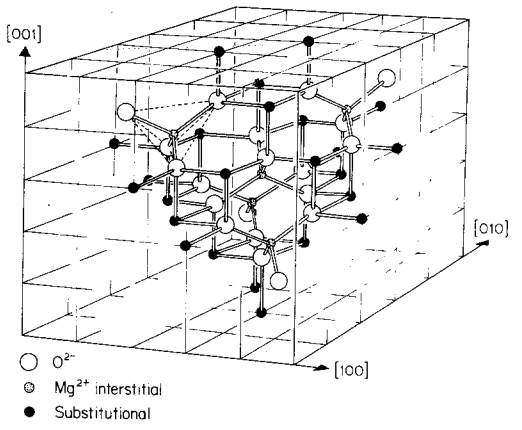

Figure 9 The 24-5 cluster.

only slightly more negative than that of the "8-2" cluster and is substantially less negative than the energies of the other spinel-like groupings. In an attempt to investigate this, an alternative configuration of the same number of octahedral impurities was tried, in which some of the trivalent aluminium ions were placed further from the centre of symmetry: at [0.5, −0.5, 1.5] and [1.5, 1.5, 2.5] rather than [0.5, −0.5, 1.5] and [−0.5, 0.5, −2.5] as in the original arrangement (Table VII). The calculation showed the cluster stability to be considerably enhanced by this modification, yielding a binding energy which is virtually the same as the inverse structure. This observation raises an important point regarding the techniques used; namely, that the arrangement of compensating octahedral cations can significantly affect the binding energy of the defect. It is possible, for example, that a lower symmetry configuration exists which is more stable than those considered in this study. The present results indicate, however, that reasonable changes in either the impurity configuration or the cation–anion repulsive potentials are unlikely to alter the basic observation that large vacancy–impurity aggregates – particularly spinel-like complexes – are energetically stable relative to simple associates and isolated point defects.

Although observations of cluster formation in magnesia are indirect and sketchy, the existence of such large stable groupings of solutes and vacancies is consistent with some experimental data. In particular, the work of Wertz and Auzins [13] and Woods and Fine [14] suggests that aggregates form in the temperature range of 400 to 500° C. Working with undoped, commercially available crystals which presumably did not contain more than 100 ppm of chromium, Wertz and Auzins further inferred the dissociation of clusters involving chromium at about 700° C. Crude calcuations for the clusters considered here, discussed in Appendix 2, are in accord with these observations, showing an orders-of-magnitude increase in the number of clusters as the temperature is lowered below 1000° C. In this sense the results given here support what many workers have long suspected: that aggregates may play a significant role in determining the crystal defect structure at the low homologous temperatures at which precipitation begins to occur.

TABLE VIII Energies of motion

Process	Relative energy (eV)
$(Mg^{x}_{Mg}-V''_{Mg})''_{1\,1\,0} \rightarrow$ (A.C.)*	2.00
$(O^{x}_{0}-V_{0})^{\cdot\cdot}_{1\,1\,0}$	2.01
$(Fe^{x}_{Mg}-V''_{Mg})''_{1\,1\,0} \rightarrow$ (A.C.)	1.58
$(Fe^{\cdot}_{Mg}-V''_{Mg})'_{1\,1\,0} \rightarrow$ (A.C.)	1.67
$(Al^{\cdot}_{Mg}-V''_{Mg})'_{1\,1\,0} \rightarrow$ (A.C.)	2.71

*Activated complex.

4.4. Energies of motion

Catlow *et al.* [2] calculated the activation energies of motion for Mg^{2+} and O^{2-} in the magnesia lattice. They assumed a simple symmetric saddle point between two anions for motion along a ⟨110⟩ direction. The starting configuration is thus a ⟨110⟩ dimer. The same procedure was followed here in the calculation of energies of motion for impurities, and the results of these calculations, as well as a recalculation of the energies of motion for Mg^{2+} and O^{2-}, are given in Table VIII. These values are sensitive to the impurity–oxygen repulsive potential, and since the iron potential is probably weak, we believe the calculated activation energy for iron is too low.

5. Summary and conclusions

The major difficulty associated with the meaningful calculation of the energies of interaction between ionic solutes and the MgO host lattice is clearly the proper choice of the solute–oxygen repulsive potential. Unlike the case of a pure crystal, reliable repulsive parameters for a solute cannot be obtained directly, and our assumption has been that the parameters are the same as those of the pure solute compound, if these are known In the absence of such information one must resort to either *ad hoc* scaling procedures or the

direct calculation of Born–Mayer parameters from a consideration of the interactions between free ions. The latter, particularly Hartree–Fock calculations, may yield poor results [35].

The assessment of the validity of an impurity potential must depend upon comparison with either potentials of known reliability for similar ions or with experimentally characterized impurity behaviour. Thus, on the basis of comparisons with the Mg^{2+}–O^{2-} interactions and the experimental heat of solution of alumina in magnesia, it seems that the choice of Born–Mayer terms used here for the Al^{3+}–O^{2-} interaction is a reasonable one, and some confidence may be placed in the results of these calculations insofar as they apply quantitatively to the behaviour of the aluminium ion in solution in MgO. In contrast, the calculated heat of solution for Fe^{3+} indicates that the repulsive potential used is too weak. However, relatively minor changes in the substitutional energy would be required to correct this, so that the potential is not grossly deficient. Although the repulsive parameters used here are not correct for a quantitative description of the behaviour of Fe^{3+} and Fe^{2+} in MgO, together with those for Al^{3+} they are representative of a range of behaviour characteristics of impurities whose interactions with the host lattice may be described as ionic. Within this range, the trends observed in the relative stability of the various defect associates are independent of the variations in the impurity–oxygen repulsive potential, so that improvements in the description of the impurity ion are unlikely (within the framework of HADES) to alter the qualitative conclusions of this work.

The calculated energies are, of course, subject to uncertainty, and it is difficult to make meaningful error estimates. However, the relative energies do not vary radically, changing by about 20% with a substantial change in the repulsive potential. This variation is probably representative. The absolute energies are least reliable, but they are also less important as far as the present work is concerned.

Taken as a whole, then, this work leads to several conclusions concerning the interactions among point defects in MgO.

(1) Impurity–vacancy dimers and trimers are energetically stable, trimers more so than dimers. Of the two possible dimer orientations in the MgO lattice, the ⟨100⟩ orientation is more stable by 0.2 to 0.4 eV due to the large displacement and polarization of the central oxygen ion. This result is the opposite of that expected on the basis of a simple monopole interaction between the defects. The neutral linear ⟨100⟩ trimer is likewise more stable than its ⟨110⟩ counterpart by 0.4 to 0.8 eV. The binding energies and the displacement fields show that the linear trimers are essentially two dimers end-to-end, sharing a common vacancy.

(2) Complex associates of impurities and vacancies, based on a "spinel-like" unit consisting of a cation interstitial tetrahedrally co-ordinated by anions and cation vacancies, are energetically more stable than simple dimers, trimers and isolated defects, becoming increasingly so as the size of the cluster increases. The large binding energy of these groupings relative to the simpler dimers and trimers indicates that clustering should be an important phenomenon at low homologous temperatures.

(3) Interstitial formation energies in MgO are large (> 10 eV) but are substantially reduced by the presence of adjacent cation vacancies, as occurs in cluster formation.

(4) Activation energies of motion for impurities are of the order of 2 eV.

To the extent that these results are consistent with the existence of a variety of impurity–vacancy associates, they are in agreement with the bulk of experimental data. The greater stability of the ⟨100⟩ dimer/trimer orientation relative to its ⟨110⟩ counterpart is in accord with the universal observation that centres having ⟨100⟩ symmetry are more prevalent than those with ⟨110⟩ symmetry, although unknown entropy terms may also be important in this regard. Quantitative comparison is practically impossible because of the lack of a firm body of experimental data. The single study [12] available which addresses itself to the problem of determining the dimer/trimer binding energies interprets the greater concentration of ⟨100⟩ orientation defects in terms of a large entropy term, but the evidence supporting this conclusion is rather weak. The energies calculated provide a self-consistent set of values which clearly indicate a hierarchy of defect structures and which permit a realistic comparison with experiment.

Acknowledgements

This research was supported by the US Department of Energy under contract No. EY-76-S-02-2390. The authors express their gratitude to Marshall Stoneham of the Theoretical Physics division of

the Atomic Energy Research Establishment, Harwell for making the HADES program available to perform this study. Michael Norgett, also of the Theoretical Physics division at Harwell, gave generously of his time to instruct one of the authors (WHG) in the use of HADES and to discuss and clarify many of the results. His invaluable help is gratefully acknowledged.

Appendix 1. Heats of solution of Al_2O_3 and Fe_2O_3 in MgO from phase diagram data

For a simple binary system, the maximum solubility of one component in a large amount of another is given by the familiar relation [49]

$$\ln(X''_A) = \frac{\Delta S^{EX}}{k} - \frac{\Delta H}{kT} \quad (3)$$

where X''_A is the maximum solubility of A in B, and where any solubility of B in A has been neglected. This relationship may be applied to ceramic systems involving aliovalent constituents to obtain an empirical description of the solubility as a function of temperature. In the present context, however, the energy change of a particular solution process

$$R_2O_3 \xrightarrow{MgO} 2R^{\cdot}_{Mg} + V''_{Mg} + 3O^x_0 \quad \Delta E_s \quad (4)$$

is desired. Extracting an estimate of such an energy change from solubility data is complicated by the existence of a solute-induced defect structure which changes with temperature and solute concentration. Thus at low concentrations or high temperatures, one expects the solute to be predominantly unassociated. In contrast, at lower temperatures and higher concentrations, significant association should occur. A proper evaluation of the energy change of a particular process requires that the defect structure be known precisely over the range of solid solubility data. This is not the case for either alumina (Al_2O_3) or hematite (Fe_2O_3). Data for Al_2O_3 have been obtained only for temperatures in excess of $\sim 1700^\circ$ C [50], with a maximum solubility of $\sim 8\%$ occurring at the eutectic temperature of 1995° C. The combination of high solubility and high temperature suggests a mixed mode of solution, a conjecture supported by calculations using available computer programs [16]. In contrast, Fe_2O_3 is very soluble in MgO at lower temperatures [51], and significant association of the ferric ion into neutral trimers occurs for iron concentrations greater than $\sim 2\%$ [16]. Given present data and the uncertainties concerning the defect configuration, the energy change for the process (4) can at best be bracketed between an upper limit derived under the assumption of complete dissociation of the solute and a lower limit derived from the same data assuming complete association into neutral trimers. Although this approach is crude, it allows a comparison with the theoretical values calculated from the HADES results.

The process of interest is*

$$Al_2O_3 \xrightarrow{MgO} (Al_2O_3)_{ss} \quad \Delta H_1 \approx \Delta E_1 \quad (5)$$

where $(Al_2O_3)_{ss}$ denotes alumina in solid solution in magnesia. Both alumina and hematite form intermediate spinels with MgO, so Reaction 5 may be split into two processes:

$$Al_2O_3 + MgO \rightarrow MgAl_2O_4 \quad \Delta H_2 \approx \Delta E_2 \quad (6)$$

$$MgAl_2O_4 \xrightarrow{MgO} (Al_2O_3)_{ss} \quad \Delta H_3 \approx \Delta E_3, \quad (7)$$

so that $\Delta E_1 = \Delta E_2 + \Delta E_3$. ΔE_2, however, is small [52] so that for the purposes of this simple calculation, $\Delta E_1 \approx \Delta E_3$. With this approximation, Reaction 4 becomes, assuming complete dissociation,

$$MgAl_2O_4 \xrightarrow{MgO} MgO + 2Al^{\cdot}_{Mg} + V''_{Mg} + 3O^x_0 \quad (8)$$

for which

$$\Delta G - \Delta G^0 = \Delta H - T\Delta S. \quad (9)$$

One may write for Reaction 8

$$\frac{a_{MgO}a_0^3a_{Al}^2a_v}{a_{MAO}} = \exp\left(\frac{\Delta G - \Delta G^0}{kT}\right). \quad (10)$$

Now, $a_{MgO} = 1$ and $a_{MAO} = 1$ since MgO and $MgAl_2O_4$ are "pure" substances. Furthermore, assuming Henry's law to hold for aluminium in the region of solid solution,

$$a_{Al} = \gamma X_{Al} \quad (11)$$

where X_{Al} is the site fraction of aluminium. The standard state for vacancies is customarily taken to be at infinite dilution so that

$$a_v = X_v = \tfrac{1}{2}X_{Al}. \quad (12)$$

*For brevity, Al_2O_3 and Fe_2O_3 will be considered to be entirely analogous here, despite the variable oxidation state of iron and its greater solubility in MgO in air.

Hence, Reaction 10 becomes

$$a_0^3 \frac{\gamma^2}{2} X_{Al}^3 = \exp\left(\frac{\Delta G - \Delta G^0}{kT}\right). \quad (13)$$

The standard free energy change for Reaction 8, ΔG^0, may be written

$$\Delta G^0 = \mu^0_{MgAl_2O_4}(ss) - \mu^0_{MgAl_2O_4} = 0, \quad (14)$$

where the standard state for aluminium in solid solution has been taken to be spinel. Now,

$$a_0 = 1 \quad (15)$$

so that Reaction 13 becomes

$$\frac{\gamma^2}{2} X_{Al}^3 = \exp\left(\frac{\Delta G}{kT}\right). \quad (16)$$

When $X_{Al} = X'_{Al}$, the solubility limit, $\Delta G = 0$ and

$$\frac{\gamma^2}{2} X'^3_{Al} = 1, \quad (17)$$

or

$$\frac{\gamma^2}{2} = \frac{1}{X'^3_{Al}}. \quad (18)$$

Thus Equation 16 becomes

$$\frac{X_{Al}^3}{X'^3_{Al}} = \exp\left(\frac{\Delta G}{kT}\right). \quad (19)$$

For an ideal solution,

$$\tfrac{1}{2} X_{Al}^3 = \exp\left(-\frac{\Delta S^{ideal}}{K}\right), \quad (20)$$

since $\Delta H^{ideal} = 0$. Hence with Equation 19 one obtains

$$\ln X'_{Al} = -\frac{\Delta G^{xs}}{3kT} = \frac{\Delta S^{xs}}{3k} - \frac{\Delta H}{3kT}, \quad (21)$$

where $\Delta G^{xs} = \Delta G - \Delta G^{ideal}$ and the factor of 2 has been absorbed into ΔS^{xs}. A plot of X'_{Al} versus $1/T$ will have a slope of $\Delta H_1/(3k)$. Enthalpies calculated for Al_2O_3 and Fe_2O_3 on the basis of Equation 21 are given in Table IX. The effects of mutual solubility may be taken into account by noting that for MgO dissolved in $MgAl_2O_4$, the spinel will obey Raoult's law approximately, so if X'_{MAO} is the mole fraction of spinel at the spinel-two phase boundary,

$$a_{MAO} = X'_{MAO} \quad (22)$$

so that Equation 17 yields $\gamma^2/2 = X'_{MAO}/X^3_{Al}$. This correction is small, however (Table IX) and, given the crudeness of the calculation, is ignored here.

For full association into trimers (of unspecified orientation) the solution process is

$$MgAl_2O_4 \xrightarrow{MgO} MgO + (Al^{\cdot}_{Mg} - V''_{Mg} - Al^{\cdot}_{Mg})^x, \quad (23)$$

for which

$$\frac{a_{Al-V-Al}}{a_{MAO}} = A \exp\left(\frac{\Delta G' - \Delta G^0}{kT}\right), \quad (24)$$

where A is a configurational pre-exponential. Here

$$\Delta G' = \Delta G + \Delta E, \quad (25)$$

where E is the energy change for the association process:

$$2Al^{\cdot}_{Mg} + V''_{Mg} \rightarrow (Al^{\cdot}_{Mg} - V''_{Mg} - Al^{\cdot}_{Mg})^x. \quad (26)$$

Proceeding as for the case of complete dissociation, with $a_{MAO} = 1$ and noting that $a_{Al-V-Al} = \gamma' X_{Al}$ one obtains the result

$$\ln X'_{Al} = -\frac{\Delta G^{xs}}{kT}, \quad (27)$$

where various constants have been absorbed into $\Delta S^{xs}/k$.

Thus, assuming complete association, a plot of $\ln X'_{Al}$ versus $1/T$ will have a slope of $\Delta H'/(kT)$, where $\Delta H'$ is now the enthalpy change for Reaction 23. The energy change for Reaction 4 is then $\Delta H' - \Delta E$. Although ΔE is not known precisely, it may be estimated conservatively as -1.5 eV based on the HADES calculations. Using this value, the lower limits given in Table IX may be obtained.

TABLE IX Estimated energy change for the process $R_2O_3 \rightarrow 2R^{\cdot}_{Mg} + V''_{Mg} + 3O^x_0$

Solute	E(eV)	From HADES
Al_2O_3	7.8(8.4)*	8.2 ± 3
	4.1	
Fe_2O_3	6.0	− 2.9 ± 3
	3.5	

* Includes a correction for mutual solubility.

Appendix 2. Estimates of the concentration of larger clusters

Although it is, in principle, possible to calculate exactly the concentration of various defect configurations interrelated by mass action expressions, it is, in practice, difficult to include large clusters. Available computer programs [16] solve a set of non-linear simultaneous equations involving the mass-action equilibrium constants. The variables in the system are chosen so as to make the iteration

as efficient as possible, and in most instances the unassociated cation vacancy and impurity concentrations provide satisfactory results. The problems in dealing with larger clusters become apparent, however, when one considers the formation of, for example, an (8-2-Al) cluster from the unassociated defects

$$8Al_{Mg}^{\cdot} + 4V_{Mg}'' + 2Mg_{Mg}^{x} \rightarrow (8\text{-}2\text{-}Al) \quad (28)$$

for which, taking the configurational pre-exponential to the 10*

$$\frac{[(8\text{-}2\text{-}Al)]}{[Al_{Mg}^{\cdot}]^8[V_{Mg}'']^4} = K'_{CL8} = 10\exp\left(\frac{8.93}{kT}\right) \quad (29)$$

Because of the large exponents in the denominator of Equation 29, K'_{CL8} must be large if a significant number of clusters are to form. This will occur at low temperatures. However, at $T = 500°$ C, $K'_{CL8} = 1.7 \times 10^{59}$, near the limit of available computer systems† which cannot handle numbers larger than $\sim 10^{76}$. For larger groupings, such as the (24-5-Al) one has (for the least stable cluster, assuming a pre-exponential of 1)

$$\frac{[(24\text{-}5\text{-}Al)]}{[Al_{Mg}^{\cdot}]^{22}[V_{Mg}'']^{11}} = \exp\left(\frac{25.3}{kT}\right), \quad (30)$$

which is greater than 10^{100} at 1000° C. Thus the problem becomes intractable when the cluster includes more than just a few impurities and vacancies.

While an exact calculation is not feasible with existing facilities, one can obtain an approximate solution sufficient to demonstrate the possible importance of large clusters at low temperatures. The formation of the (8-2-Al) cluster from ⟨100⟩ trimers can be written as

$$4(Al_{Mg}^{\cdot}\text{–}O\text{–}V_{Mg}''\text{–}O\text{–}Al_{Mg}^{\cdot})^{x} \rightarrow (8\text{-}2\text{-}Al) \quad (31)$$

for which

$$\frac{[(8\text{-}2\text{-}Al)]}{[(Al_{Mg}^{\cdot}\text{–}O\text{–}V_{Mg}''\text{–}O\text{–}Al_{Mg}^{\cdot})^{x}]^4} = K_{CL8} = \frac{10}{3^4}\exp\left(\frac{2.21}{kT}\right). \quad (32)$$

Now, exact calcuations which do not include large clusters indicate that at temperatures of ~400° C and solute levels as low as 200 ppm, 89% or more of the trivalent solutes are associated into ⟨100⟩ trimers. This fraction will increase with increasing solute concentration (~96% at 1000 ppm) as well as with increasing trimer binding energies and pre-exponentials. In the present approximation it will be assumed that virtually all the solute is bound into trimers at low temperatures. If one introduces larger, energetically more stable groupings, they will form at the expense of the trimers. Defining $X_{CL8} = [(8\text{-}2\text{-}Al)]$, $X_T = [(Al_{Mg}^{\cdot}\text{–}O\text{–}V_{Mg}''\text{–}O\text{–}Al_{Mg}^{\cdot})^{x}]$ and [Al] = total solute fraction, then the solute conservation equation may be approximated as

$$[Al] \approx 2X_T + 8X_{CL8} \quad (33)$$

in the temperature range of interest. Substituting into Equation 32, one obtains

$$\frac{X_{CL8}}{\frac{1}{2}([Al] - 8X_{CL8})^4} = K_{CL8} \quad (34)$$

or

$$4K_{CL8}^{1/4}X_{CL8} + X_{CL8}^{1/4} = \tfrac{1}{2}[Al]K_{CL8}^{1/4}. \quad (35)$$

Table X gives the values of K_{CL8} calculated from

TABLE X Estimates of the concentration of 8–2–Al clusters

Temperature (°C)	Al(ppm)	K_{CL8}	X_{CL8}	Fraction of solute in cluster
400	200	4.38×10^{15}	2.288×10^{-5}	0.915
700	200	3.46×10^{10}	2.336×10^{-6}	0.093
1000	200	6.94×10^{7}	6.948×10^{-9}	2.779×10^{-6}
400	1000	4.38×10^{15}	1.218×10^{-4}	0.974
700	1000	3.46×10^{10}	7.165×10^{-5}	0.573
1000	1000	6.94×10^{7}	3.830×10^{-6}	0.031

*The concentration of large groupings is best defined as the number per unit volume. The concentration which appears in Equation 29, however, is a site fraction. The statistical analysis leading to a rigorous definition of [(8-2-Al)] in terms of the volume concentration is made complicated by the fact that each cluster occupies many cation sites. However, as long as the concentration of clusters per unit volume, C_{CL8}, is much less than the total number of cation sites per unit volume, N, ($C_{CL8} \ll N$), then $[(8\text{-}2\text{-}Al)] \approx C_{CL8}/N$.

†IBM 370.

TABLE XI Estimates of the concentration of (24–5–Al) clusters

Temperature (°C)	Al(ppm)	K_{CL}	X_{CL}	Fraction of solute in cluster
400	200	5.86×10^{67}	9.069×10^{-6}	0.997
700	200	1.80×10^{45}	6.721×10^{-6}	0.740
1000	200	2.255×10^{33}	2.255×10^{-11}	2.481×10^{-6}
400	1000	5.86×10^{67}	4.543×10^{-5}	0.999
700	1000	1.80×10^{45}	4.265×10^{-5}	0.938
1000	1000	2.255×10^{33}	1.475×10^{-5}	0.325
1200	1000	1.29×10^{28}	6.310×10^{-9}	1.39×10^{-4}

Equation 35 at 400, 700 and 1000° C for solute levels of 200 and 1000 ppm. At 1000° C, the approximation (33) does not hold, and significant numbers of solute atoms will be unassociated as well as distributed among the dimer/trimer configurations. Thus, at temperatures above 700° C, K_{CL8} represents a significant overestimate. Nevertheless, it is apparent that significant numbers of clusters may be expected to form in a temperature range of 400 to 700° C at solute levels as low as 200 ppm, increasing rapidly as the solute concentration is increased.

The expression for (24-5-Al) clusters analogous to Equation 35 is:

$$11K_{CL}^{1/11}X_{CL} + X_{CL}^{1/11} = \tfrac{1}{2}[\mathrm{Al}]K_{CL}^{1/11}. \quad (36)$$

Using the most stable form of this cluster, and assuming a configurational pre-exponential of 1, $K_{CL} = (1/3^{11}) \exp(9.75/kT)$, and one may calculate the results given in Table XI. The trends are analogous to those for the (8-2-Al) cluster. It should be re-emphasized, however, that these are crude estimates and are meant only to indicate that cluster formation, as described within the HADES model, is a plausible equilibrium process in MgO at low temperatures.

Appendix 3. Intrinsic defects

The energies of several intrinsic defect structures were investigated briefly. These included the divacancy, multiple vacancy associates and interstitials.

Catlow *et al.* [2] calculated the formation energy of the divacancy. The calculation was repeated here and the binding energy relative to the separated vacancies is given in Table XII. It is of interest to note that the binding energy calculated by HADES (− 2.67 eV) is virtually the same as that calculated using a simple coulomb expression,

$$E_b = -\frac{4e^2}{\epsilon r_0} (\approx -2.75\ \mathrm{eV}), \quad (37)$$

where ϵ is the macroscopic static dielectric constant for MgO (9.7). The ionic displacements and polarizations of the divacancy, however, correspond essentially to a superposition of the displacements and polarizations of each separated vacancy. Evidently the polarization of the surrounding medium is virtually the same as it would be if there were matter between the vacancies. Since ϵ accounts for the effects of the polarization on the field at a given point in the solid, it is perhaps not surprising that Equation 37 should hold as well as it does in this case.

Two larger clusters of vacancies were investigated in addition to the simple divacancy. The "4-vacancy is simply a {1 0 0} planar arrangement of two divacancies. This grouping was also considered by Stewart and Mackrodt [53, 54] in their studies of the interactions between sur-

TABLE XII Intrinsic defect energies

Process	Energy (eV)	Remarks
$Mg_{Mg}^{x} \rightarrow Mg_{\infty}^{2+} + V_{Mg}''$	23.83	
$O_O^x \rightarrow O_\infty^{2-} + V_O^{\cdot\cdot}$	24.70	
$\mathrm{null} \rightarrow V_{Mg}'' + V_O^{\cdot\cdot}$	7.7	Schottky energy
$V_{Mg}'' + V_O^{\cdot\cdot} \rightarrow (V_{Mg}'' - V_O^{\cdot\cdot})^x$	− 2.67	− 1.34 eV per vacancy; − 2.75 eV expected from coulomb calculation
$2V_{Mg}'' + 2V_O^{\cdot\cdot} \rightarrow (4\text{-vacancy})^x$	− 8.39	− 2.10 eV per vacancy
$4V_{Mg}'' + 4V_O^{\cdot\cdot} \rightarrow (8\text{-vacancy})^x$	− 21.28	− 2.66 eV per vacancy
$Mg_{Mg}^{x} \rightarrow Mg_i^{\cdot\cdot} + V_{Mg}''$	12.42	
$O_O^x \rightarrow O_i'' + V_O^{\cdot\cdot}$	12.1	

faces and point defects in cubic ionic crystals. Their findings are in agreement with those reported here. The "8-vacancy" is the obvious cubic arrangement of two 4-vacancies. The striking feature of the results is the magnitude of the binding energies per vacancy. It can be easily shown [35] that the limiting value for this binding energy is $-1/2 g_s$ (-3.85 eV) where g_s is the Schottky energy. Apparently the initial approach to this limit is rapid, since for only eight vacancies the binding energy is 70% of the limiting value. Energetically speaking, clusters of vacancies much larger than the 8-vacancy may be considered to be macroscopic voids rather than microscopic associates of point defects. A simple calculation suffices to show that, like the divacancy, these larger groupings of vacancies will not form in significant numbers as intrinsic defects in MgO at temperatures lower than the melting point. If a supersaturation of vacancy pairs is produced via an extrinsic mechanism such as irradiation or reduction of OH^-, however, clusters could form in sufficient quantities to become important in void formation. In this limited sense, the present observations are in accord with the suggestion of Briggs [55, 56] and Briggs and Bowen [57] that large cavities in MgO may be due to the coalescence of microcavities.

The interstitial formation energies for Mg^{2+} and O^{2-} given in Table XII preclude their formation in the MgO lattice. However, it should be noted that these energies are those for the reaction:

$$Mg^{x}_{Mg} \rightarrow Mg^{\cdot\cdot}_{i} + V''_{Mg} \qquad (38)$$

when the interstitial and vacancy are widely separated. In contrast, as a part of a cluster of vacancies, the cation interstitial becomes a stable defect, as discussed in the main text. Whether there is some configuration which would lower the energy sufficiently to admit interstitials as intrinsic defects is uncertain, but seems unlikely in view of the large energies given in Table XII. It is noteworthy that the interstitial energy for O^{2-} is slightly less than that for Mg^{2+}, the opposite of what one would guess solely on the basis of ionic size, Dienes *et al.* [40] obtained a similar result for octahedral interstitials in alumina. If one thinks in terms of ionic radii, this result is counter-intuitive, given the large radius of the oxygen ion (1.4 Å) and the small size of the tetrahedral "hole" ($r \approx 0.4$ Å). For an ionic material, however, such concepts may be misleading. The high charge of an interstitial ion polarizes the lattice and strongly repels like ions. These effects, together with the close proximity of ions of opposite charge, lowers the overall energy of the configuration. Although the repulsive term is a substantial part of the total defect energy, the final, relaxed state is determined to a considerable extent by electrostatic interactions. Since the absolute value of the charge is the same for the oxygen and magnesium ions, the similarity of their interstitial energies, within the framework of HADES, is perhaps not surprising. It should be noted that while the interstitial energies are very sensitive to the Mg^{2+}–O^{2-} repulsive potential, they are much less dependent upon the Mg^{2+}–Mg^{2+}, O^{2-}–O^{2-} potentials since the long-range coulombic repulsion pushes like ions so far apart.

References

1. J. GOVINDARAJAN, P. W. M. JACOBS and M. A. NERENBERG, *J. Phys. C: Solid State Phys.* **9** (1976) 3911; **10** (1977) 1809.
2. C. R. A. CATLOW, I. D FAUX and M. J. NORGETT, *ibid* **9** (1976) 419. (Also published as AERE Harwell report TP569.)
3. J. E. WERTZ and P. V. AUZINS, *Phys. Rev.* **139** (1965) A1645.
4. W. C. O'MARA. J. J. DAVIES and J. E. WERTZ, *ibid* **179** (1969) 816.
5. Y. CHEN, M. M. ABRAHAM, L. C. TEMPLETON and W. P. UNRUH, *ibid* **B11** (1975) 881.
6. A. M. GLASS and T. M. SEARLE, *J. Chem. Phys.* **46** (1967) 2092.
7. B. HENDERSON and T. P. P. HALL, *Proc. Phys. Soc.* **90** (1967) 511.
8. W. LOW, *Phys. Rev.* **105** (1957) 801.
9. J. E. WERTZ and P. V. AUZINS, *ibid* **106** (1957) 484.
10. J. H. E. GRIFFITHS and J. W. ORTON, *Proc. Phys. Soc. (London)* **73** (1959) 948.
11. G. F. IMBUSCH, A. L. SCHAWLOW, A. D. MAY and S. SUGANO, *Phys. Rev.* **140** (1965) A830.
12. A. M. GLASS, *J. Chem. Phys.* **46** (1967) 2080.
13. J. E. WERTZ and P. V. AUZINS, *J. Phys. Chem. Solids* **28** (1967) 1557.
14. K. N. WOODS and M. E. FINE, *J. Amer. Ceram. Soc.* **52** (1969) 186.
15. J. J. DAVIES, S. R. P. SMITH and J. E. WERTZ, *Phys. Rev.* **178** (1969) 608.
16. W. H. GOURDIN, W. D. KINGERY and J. M. DRIEAR, *J. Mater. Sci.* **14** (1979) 2074.
17. J. S. THORP, R. A. VASQUEZ, C. ADCOCK and W. HUTTON, *ibid* **11** (1976) 89.
18. J. E. WERTZ, J. W. ORTON and P. AUZINS, *J. Appl. Phys.* **335** (1962) 332.
19. B. HENDERSON, J. E. WERTZ, T. P. P. HALL and R. D. DOWSING, *J. Phys. C: Solid State Phys.* **4** (1971) 107.
20. W. UNRUH, Y. CHEN and M. M. ABRAHAM, *Phys. Rev. Letters* **30** (1973) 446.
21. J. E. WERTZ, P. AUZINS, J. H. E. GRIFFITHS and

J. W. ORTON, *Discuss. Faraday Soc.* **28** (1959) 136.
22. J. E. WERTZ, G. SAVILLE, P. AUZINS and J. W. ORTON, *J. Phys. Soc. Jap. Suppl. II* **18** (1963) 305.
23. B. J. WUENSCH, in "Mass Transport Phenomena in Ceramics", edited by A. R. Cooper and A. H. Heuer (Plenum, New York, 1975).
24. W. P. WHITNEY and V. S. STUBICAN, *J. Amer. Ceram. Soc.* **54** (1971) 349.
25. A. M. GLASS and T. M. SEARLE, *J. Chem. Phys.* **48** (1968) 1420.
26. G. W. WEBER, W. R. BITLER and V. S. STUBICAN, *J. Amer. Ceram. Soc.* **60** (1977) 61.
27. B. G. DICK and A. W. OVERHAUSER, *Phys. Rev.* **112** (1958) 90.
28. A. D. B. WOODS, W. COCHRAN and B. N. BROCKHOUSE, *ibid* **119** (1960) 980.
29. M. J. NORGETT, AERE report R.7650 (January 1974).
30. *Idem*, AERE report R.7780 (July 1974).
31. *Idem*, AERE report R.7015 (1972).
32. M. J. NORGETT and R. FLETCHER, *J. Phys. C: Solid State* **3** (1970) L190.
33. C. H. WOO and M. P. PULS, to be published.
34. *Idem*, to be published.
35. W. H. GOURDIN, Ph.D. dissertation, MIT (1977).
36. C. R. A. CATLOW, Ph.D. thesis, University of Oxford (1974).
37. C. R. A. CATLOW and M. J. NORGETT, *J. Phys. C: Solid State Phys.* **6** (1973) 1325.
38. C. H. WOO, M. P. PULS and M. J. NORGETT, *J. Physique, Colloq.* (Berlin Conference) (September 1976).
39. M. J. L. SANGSTER, G. PECKHAM and D. H. SAUNDERSON, *J. Phys. C.: Solid State Phys.* **3** (1970) 1026.
40. G. J. DIENES, D. O. WELCH, C. R. FISCHER, R. D. HATCHER, O. LAZARETH and M. SAMBERG, *Phys. Rev.* **B11** (1975) 3060.
41. P. T. WEDEPOHL, *Proc. Phys. Soc.* **92** (1967) 79.
42. C. R. A. CATLOW and B. E. F. FENDER, *J. Phys. C: Solid State Phys.* **8** (1975) 3267 (Also published as AERE report TP. 604).
LINNETT, *Trans. Farad. Soc.* **64** (1968) 1489.
44. R. D. SHANNON and C. T. PREWITT, *Acta Cryst. B* **25** (1969) 925.
45. J. SHERMAN, *Chem. Rev.* **11** (1932) 93.
46. T. C. WADDINGTON, in "Advances in Inorganic Chemistry and Radiochemistry", Vol. 1, edited by H. J. Emeleus and A. G. Sharpe (Academic Press, New York, 1959) p. 157.
47. M. F. C. LADD and W. H. LEE, "Progress in Solid State Chemistry", Vol. 1, edited by H. Reiss MacMillan, New York, 1964) p. 37.
48. P. GEORGE and D. S. McCLURE, in "Progress in Inorganic Chemistry", Vol. 1, edited by F. A. Cotton, (Interscience, New York, 1959) p. 389.
49. R. A. SWALIN, "Thermodynamics of Solids", 2nd edn. (Wiley, New York, 1972).
50. A. M. ALPER, R. N. McNALLY, P. H. RIBBE and R. C. DOMAN, *J. Amer. Ceram. Soc.* **45** (1962) 263.
51. H. S. ROBERTS and H. E. MERWIN, *Amer. J. Sci.* **21** (1931) 145.
52. A. NAVROTSKY, in "International Review of Science. Transition Metals Part I: Inorganic Chemistry Series Two" Vol. 5, edited by D. W. A. Sharp, 29ff.
53. W. C. MACKRODT and R. F. STEWART, *J. Phys. C. Solid State Phys.* **10** (1977) 1431.
54. R. F. STEWART and W. C. MACKRODT, *J. Phys. (Paris) Colloq.* **7** (1976) 247.
55. A. BRIGGS, *J. Mater. Sci.* **10** (1975) 729.
56. *Idem, ibid* **10** (1975) 737.
57. A. BRIGGS and D. H. BOWEN, "Mass Transport in Oxides", N.B.S. publication no. 296, edited by J. B. Wactman, A. D. Franklin (1967).
58. W. D. KINGERY, H. K. BOWEN and D. R. UHLMANN, in "Introduction to Ceramics", 2nd edn. (Wiley, New York, 1976).

Received 15 August and accepted 2 October 1978.